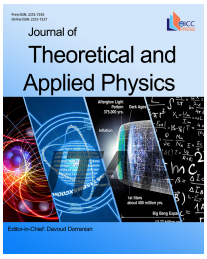

Volume 19, Issue 2, 192520 (1-12)

Journal of Theoretical and Applied Physics (JTAP)

https://doi.org/10.57647/j.jtap.2025.1902.20

Impact of applied voltage on different electrode gap for the generation of ozone

Arun Kumar Shah[1], Ram Lal Sah[1,3], Rajendra Shrestha[1,2], Bablu Kant Thakur, Saddam Husain Dhobi[1,4], Jeevan Jyoti Nakarmi[4], Lekha Nath Mishra[1,*]

[1]*Department of Physics, Patan Multiple Campus, Tribhuvan University, Lalitpur, Nepal.*
[2]*Department of Physics, Nepal Banepa Polytechnic Institute, Banepa, Kavre, Nepal.*
[3]*Padma Kanya Campus, Bagbazar, Kathmandu, Nepal.*
[4]*Central Department of Physics, Tribhuvan University, Kirtipur, Nepal.*

[*]**Corresponding author:** lekha.mishra@pmc.tu.edu.np

Original Research

Received:
31 January 2025
Revised:
25 March 2025
Accepted:
3 April 2025
Published online:
10 April 2025

Abstract:

This study investigates the influence of applied voltage and electrode gap on the efficiency of ozone generation in a plasma-based system. Ozone, as a strong oxidizing agent, plays a critical role in various industrial applications, including air and water purification. The objective of this research was to analyze the relationship between applied voltage, electrode gap, and ozone production efficiency. Discharges have been characterized with electrical methods. A plasma discharge system was constructed with electrode gap distances of 0.5 mm, 1.0 mm, and 1.5 mm. The applied voltage was varied between 9.38 kV and 17.20 kV at intervals of thirty seconds. The findings revealed a positive correlation between applied voltage and ozone concentration, with higher voltages leading to increased ozone production. Specifically, ozone concentrations ranged from 99 ppm to 786 ppm for a 0.5 mm gap, 56 ppm to 555 ppm for a 1.0 mm gap, and 20 ppm to 395 ppm for a 1.5 mm gap. The result further demonstrated that ozone production decreases as the electrode gap widens, highlighting the impact of electrode gap distance on ozone generation. Additionally, non-linear trends were observed, where ozone concentration increased moderately with smaller voltage changes and more significantly with higher voltage increments.

Keywords: Ozone production; Applied voltage; Electrode gap distance; Plasma-based systems; Ozone generation efficiency

1. Introduction

Dielectric Barrier Discharge (DBD) is a non-thermal plasma technology widely used in ozone production due to its high efficiency and scalability [1]. Coaxial DBD systems, characterized by their cylindrical geometry with a central electrode surrounded by a dielectric barrier and an outer electrode, are particularly favored for their ability to achieve uniform discharge and maintain stable operation under varying conditions [2]. The fundamental characterization of current and voltage in these systems is essential to optimize energy input and maximize ozone yield. The growing demand for ozone in applications such as water purification [3], air sterilization [4], and industrial oxidation processes [5] has driven significant interest in enhancing the efficiency of DBD systems. Ozone's strong oxidative properties make it invaluable in these fields, but its production must balance energy consumption with output to remain economically viable [6, 7]. Coaxial DBD reactors provide an effective solution, with their design allowing for precise control over the discharge process and its related parameters. Significant research has highlighted the importance of understanding electrical characteristics such as discharge current waveforms, applied voltage, and energy dynamics in coaxial DBD reactors [8]. These parameters directly influence ozone concentration, energy yield, and operational stability. Adjustments in electrode configuration, gas composition, and discharge duration have been shown to significantly impact ozone generation efficiency [9].

In the context of rising global environmental challenges and industrial demands, the advancement of coaxial DBD technology for ozone generation represents a critical area of research. A deeper understanding of current and voltage

characteristics not only aids in optimizing ozone production but also supports sustainable energy usage, making this technology increasingly significant for both scientific and practical applications [10]. The characterization of current and voltage in coaxial dielectric barrier discharge (DBD) systems plays a pivotal role in optimizing ozone production. These systems, which rely on high-voltage electrical discharges to generate ozone, have been extensively studied to understand the interplay between electrical parameters and ozone generation efficiency. Insights from such studies inform reactor design and operational strategies to enhance performance and energy efficiency. Coaxial DBD reactors typically operate at voltages of up to 18 kV and frequencies ranging from 20 kHz to 60 Hz [11]. The discharge current waveforms within these reactors provide critical information about energy dynamics and help in fine-tuning reactor configurations. Adjustments in electrode design, such as increasing the mesh number and electrode length, have demonstrated improvements in energy yield by approximately 48% [12].

Ozone generation in DBD systems is influenced by various factors, including gas composition, flow rate, and operational conditions. Oxygen, compared to air or argon, has been shown to produce higher ozone concentrations. Furthermore, humidity levels play a significant role, with increased humidity leading to enhanced ozone production [13]. The applied voltage and discharge time also directly affect ozone concentration, with higher values generally resulting in greater ozone output. However, increased gas flow rates may inversely impact ozone yield [14]. While striving to optimize DBD systems for ozone production, a balance must be maintained between energy efficiency and ozone yield. Excessive energy input does not always correlate with proportional increases in ozone generation, necessitating a careful evaluation of operational trade-offs to achieve optimal results.

Dielectric Barrier Discharge is widely employed to produce ozone for water treatment [15]. A gap between two electrodes, a single which is coated in a dielectric substance like quartz or glass, is where an electrical gas discharge occurs. Because it doesn't produce any noise when it functions, its discharge is referred to as silent. By acting as an electrical current limiter, the barrier keeps an arc or spark from forming. Understanding and maximizing the discharge process depends on variables including power, temperature, and electron density. Langmuir probes, microwave interferometers, laser Thomson scattering, as well as optical emission spectroscopy (OES) are some of the techniques available to measure these [16]. OES is preferred due to its suitability for small plasma dimensions and strong collision processes in atmospheric pressure discharge. Characterizing DBD is vital for investigating and optimizing micro-discharge properties, from small lab setups to large-scale industrial applications. This involves studying applied voltage, discharge current, power consumption, and energy dissipation during discharge formation.

Ozone, comprising three oxygen atoms, is a potent oxidizing agent that reacts with various substances like iodide and hydroxide. Its presence in the stratosphere, formed by UV-ray interaction with molecular ozone, has implications for Earth's well-being. Ozone finds valuable application in wastewater purification, particularly through industrial-scale discharge [17]. However, this process demands a substantial amount of ozone. Notably, ozonation for water treatment offers several advantages: (a) Ozone is a powerful and reactive oxidizer, (b) it eliminates the need to handle and store toxic chemicals, (c) its by-products pose no known health or environmental risks, and (d) ozone proves highly effective in eliminating bacteria, viruses, spores, and cysts [18]. Water pollution, the contamination of water bodies, severely impacts water quality, posing hazards to both the environment and human health. Ozone (O_3) is a highly reactive chemical known for its potent oxidation potential. It finds extensive industrial applications, such as sterilizing equipment, disinfecting water and food, and purifying air. Unlike other oxidants, ozone leaves no harmful byproducts [19]. Its effectiveness in destroying organic compounds and bacteria makes it crucial for water treatment. Various methods have been explored to enhance ozone production rates, with ultraviolet radiation, electrolysis, and electrical discharges being common approaches. Among these, DBD stands out for its efficiency at room temperature and pressure. In DBD, high-energy electrons collide with oxygen molecules, leading to dissociation and subsequent reformation as ozone.

$$e^- + O_2 \rightarrow O + O + e^-$$

and

$$2O_2 + O \leftrightarrow O_3 + O_2$$

Ozone processes are short-lived and reversible at ambient temperature, making them crucial for wastewater treatment. Ozone's unique ability to decompose back into oxygen ensures no residual reactions in water. Moreover, its thirteen-fold higher solubility in water compared to oxygen underscores its effectiveness. Enhanced production efficiency is imperative with growing applications and demand [20]. DBD reactors utilize alternating current to generate brief, filamentary micro-discharges over electrode surfaces. Their electrodes can be parallel plates or concentric cylinders, with the latter preferred for gas conversion due to reduced bypassing of the plasma region. DBDs are simple, scalable, and operate at atmospheric pressure and room temperature, making them suitable for industrial applications. The first used of DBD in 1857 for ozone production in water treatment setups [21]. The working gases for the DBD ozone generating are air and oxygen, and voltages between 0 and 18 kV are applied at a frequency of 50 Hz. In their work, the researchers examine how the electrode design, applied voltage, and gas flow rate affect the rates at which ozone is produced. In an experiment, three electrode lengths- 15, 23, and 31 centimeters-were used to measure flow rates, which varied from 0.25 to 4 L/min. With an applied voltage of 10 kV and an oxygen flow rate of 0.25 L/min, the highest concentration of ozone ever measured was 3700 ppmv. The findings show that, at a given voltage, ozone concentration decreases with increasing flow rates but increases with voltage. Notably, the 23 cm electrodes length produces the maximum ozone concentration for a constant the voltage being applied [22].

The electrical and optical characteristics of coaxial DBD for the atmosphere's pressure ozone generation, The discharge was examined while operating at 50 Hz frequencies and 0 to 18 kV voltages. Electron temperature (1.8 eV) as well as density (1.74×10^{17} cm^{-3}) were calculated using optical emission spectroscopy. The electron density was determined to be 2.16×10^{15} cm^{-3} employing the current density measurement method. The electrical characteristics were recorded using current and voltage, with a voltage range of 7.8 kV to 11 kV including a venturi meter to measure the gas flow rate (4.5 to 15.5 L/min). The gas flow rate and applied voltage both affected the amount of energy dissipated [23].

2. Methods and materials

Voltage-current technique

The quantification of power dissipation or consumption in the DBD process holds significant importance for researchers. Understanding the power involved is crucial to ensure proper experimental conditions and outcomes. In order to handle this crucial component, the power consumption of the DBD system was determined using two different approaches: the Lissajous curve method and the current-voltage method. These approaches were chosen to offer comprehensive insights into the energy dynamics of the DBD plasma generation. By employing these methods, a more accurate understanding of the power consumption during the DBD process is obtained, facilitating informed and effective experimental procedures. The DBD's current-voltage signals can be multiplied to determine instantaneous power usage based on electrical parameters.

$$P_i = V_i I_i \tag{1}$$

where I_i stands for the instantaneous current, P_i for the instantaneous power, and V_i for the immediate applied voltage during the discharge. One can derive the time-averaged electrical power consumption P using equation (2) [24]:

$$P = \frac{1}{T}\int_{t=0}^{T} V(t)I(t)dt = f\int_{t=0}^{T} V(t)I(t)dt \tag{2}$$

where f is the applied voltage frequency and T is the shape of the waveform period. Plotting the charge (Q) with voltage (V) curve, often known as the Lissajous curve, is another easy technique. The area within this curve represents the energy lost during each cycle of discharge. Energy dissipated with discharge per cycle multiplied by the applied source's frequency yields the electrical power [24]:

$$P = f\int_{t=0}^{T} V(t)dQ \tag{3}$$

The Lissajous curve can be used to determine the primary plasma device parameters, such as the total capacitance of the DBD (C_{total}), the capacitance of the air gap (C_g), and the capacitance of the dielectric barrier (C_d). The discharged cell can be thought of as two capacitances connected in series, one for the insulating barrier (C_d) and another for the discharge (C_g). When plasma is produced, the C_g's value varies. The parallelogram's AD along with BC sides represent the "passive or dark periods of the DBD," which are conditions when the plasma is off. There is no charge transfer via the air gap during this phase, and the slope of these two sides equals the total capacitance (C_{total}), which may be computed as the series combination of the dielectric barrier capacitance (C_d) and capacitance (C_g).

$$C_{\text{total}} = \frac{C_g C_d}{C_g + C_d} \tag{4}$$

The DC and AB sides of the parallelogram are related to plasma on condition known as "the active phases" where the slope is equal to the dielectric barrier capacitance (C_d). The discharging mechanism will be in the working mode when the value associated with the AC maximum voltage (V_m) provided to the DBD reactor is larger than the value of the beginning voltage for the micro-discharges (V_0). The reactor functions as a basic capacitor during the micro-discharge extinction period, also known as the pause discharge mode. The highest electric charge $Q_{\max}$ in this instance that travels through the external circuit from the DBD reactor is [25];

$$Q_{\max} = C_{\text{total}} V_m \tag{5}$$

where C_{total} is the reactor's total electrical capacitance. Conversely, the maximum electrical charge $Q_{\max}$ that flows through the external circuit during the active discharge mode, or the ignition time of the micro-discharges within the reactor;

$$Q_{\max} = C_d\left[V_m - \left(\frac{C_d}{C_d + C_g}\right)V_0\right] \tag{6}$$

where C_g is the electric capacitance of the discharging gap that is restricted between the reactor's electrodes, and C_d is the electric capacitance for the dielectric barriers covering the electrode surfaces. The formula is used to calculate the amount of the onset voltage V_0 needed to start the micro-discharges within air-fed DBD reactors [26];

$$V_0 = 26.55pd + 1480 \tag{7}$$

where d is the discharge gap's width, which is limited between the electrodes, and p is the air pressure passing through the reactor. The formula indicates that the electric power P used to create the micro-discharges within the DBD reactors is dependent on the ac peak voltage V_m delivered to the reactors rather than the root mean square voltages V_{rms} [26];

$$P = 4f\left(\frac{C_d^2}{C_d + C_g}\right)V_0(V_m - V_0) \tag{8}$$

where f represents the frequency of the alternating current voltage. In DBD, electric current (I) passes between electrodes across a specified plasma volume of cross section A, with no current leakage to the surrounding area. This allows the measured current to be used as an indicator for plasma created at atmospheric pressures. According to (9), the current density (J) is determined by the combination of electron density (n_e) as well as drift velocity (v_d) of electrons, which are in turn a function of electric field.

$$J = n_e e v_d \tag{9}$$

To get ne using equation (9), look up the values of v_d for various electric field levels in the literature. Alternatively, the electron density ne can be estimated using the measured applied voltage as well as average discharge current data. This method is known as the power balancing method and is explained by the following equation:

$$n_e = \frac{P_{av}}{2Av_dE_{\text{lost}}} \tag{10}$$

where P_{av} is average power, A is electrode area, v_b is Bohm velocity, while E_{lost} is the system's energy loss per electron-ion pair. In a recent investigation, the equation (10) was utilised to quantify the electron density in the argon discharge produced by parallel-plate DBD [27]. The voltage put between the electrodes was measured with a high-voltage probe, and the discharge current was determined through a shunt resistor on the discharge tube's earth side. The density of electrons in air plasma has been determined to be $n_e = 8.97 \times 10^{11}$ cm^{-3}, which is generally consistent with the measurement of electron density in low temperatures plasmas [28].

Experimental setup and ozone production

Figure 1 depicts the setup used for the experiment for the ozone generating apparatus, which utilized a dielectric barrier discharge. The experimental setup for ozone synthesis necessitated painstaking attention to detail to enable accurate measurements and control. The reactor, which measured 133.5 cm in length, was fundamental to the setup. It was strategically placed at a distance of 106.5 cm from the output of the ozone analyzer, providing for accurate ozone concentration analysis. The ozone chamber was powered by high voltage AC transformers, especially a $0-18$ kV, 50 Hz transformer labelled as NEEK. This transformer was critical in providing the high power required to start the ozone generating process within the chamber. The ozone chamber contained 14 identical DBD tubes that were accurate positioned. These tubes served as the foundation for the ozone production mechanism, allowing ozone to be produced by regulated discharge reactions.
Also, in figure 1 (a) experimental setup of ozone, 1 (b) is ozone analyzer, 1 (c) Power Supply. Air pump (SB-548 A, 3 W, flow 3.5 L/minute and 7.0 L/minute at 0.02 Mpa) was used to regulate the constant air flow. An ozone analyzer BMT 964 model was used to measure ozone concentration. This analyzer measured ozone levels in real time, providing crucial information on the efficiency and performance of the ozone production. With suitable and precious component properly chosen and fitted into the setup as shown in figure 1 was employed to generate data for valuable insights about ozone dynamics.

3. Results and discussion

Electrical characterization of ozone production coaxial DBD configuration

A plasma-based ozone production system's efficiency and effectiveness are influenced by a number of crucial configuration elements. These comprise the discharge characteristics, electrode arrangement, gas flow rate, and applied voltage. The energy transmitted to the gas during discharge is determined by the applied voltage; larger voltages generally result in increased formation of ozone, while extreme voltages may induce adverse responses. The ideal gas flow rate is determined experimentally. It impacts the efficiency of ozone formation by influencing residence time inside the discharge region. Ozone generation rates are influenced by the design and spacing of the electrodes, which also affect the dispersion of the electric field and the homogeneity of the discharge. Mode and frequency of discharges are important factors as well; dielectric barrier discharges are frequently chosen for effective ozone production. Thorough characterization methods, such as spectroscopic analysis and monitoring of ozone concentrations, are necessary to evaluate the system's performance and guarantee reliable ozone generation for various uses. Figure 1 depicts the IV characterization of ozone generation, which was obtained by [29] and is of a similar type.
Figure 2 illustrated the I-V characteristics with corresponding Lissajous figure at 1.5 mm gap at various applied voltages illustrates how the area changes with increasing voltage, reflecting the energy accumulation in the system. As the applied voltage increases from 9.38 kV to 17.20 kV, the corresponding area increases, indicating a direct relation-

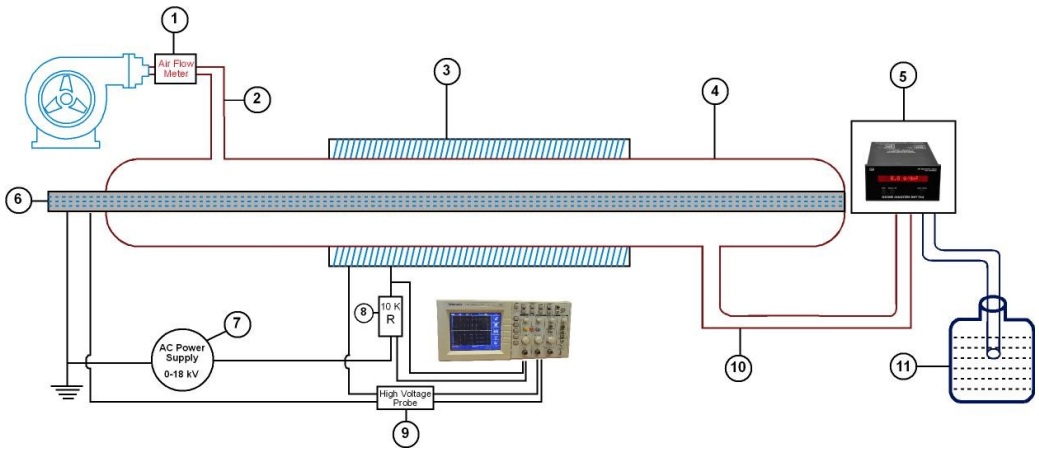

Figure 1. (1) Air pump, (2) Inlet, (3) Outer electrode, (4) Glass tube, (5) Ozone analyzer, (6) Inner electrode, (7) High voltage AC power supply, (8) Resistor (10 kΩ), (9) High voltage probe connected with digital storage oscilloscope, (10) Outlet for ozone produced, and (11) Water containing beaker.

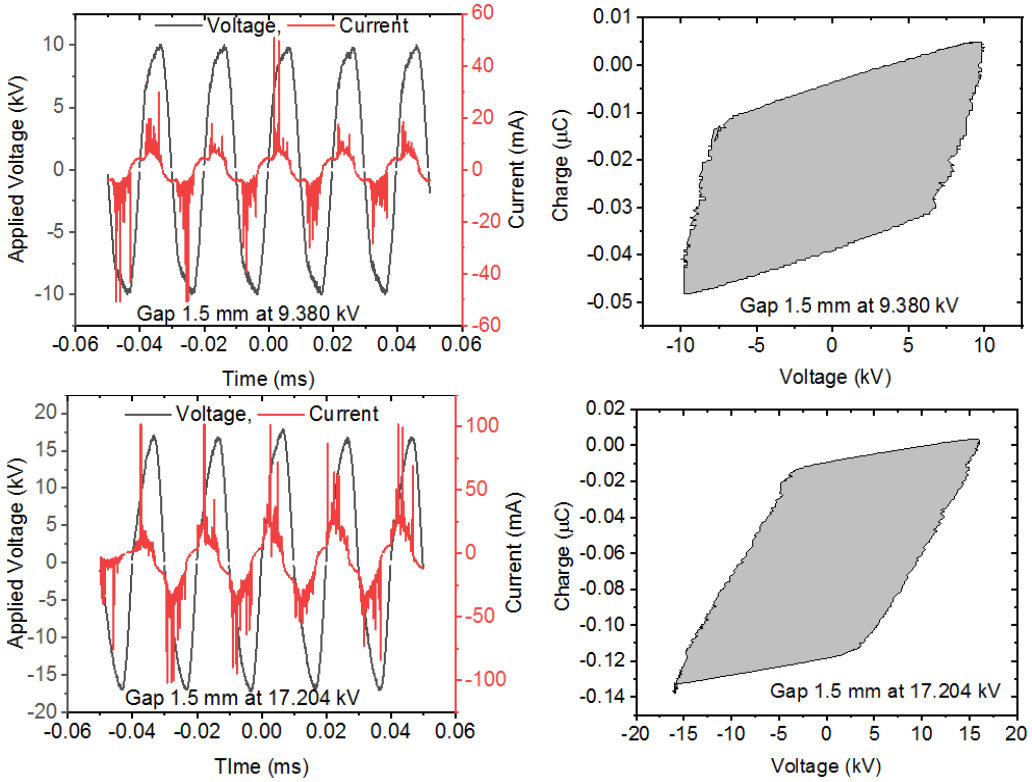

Figure 2. I-V characterization with corresponding Lissajous figure at 1.5 mm gap

ship between voltage and the extent of the area impacted by the energy. At 9.38 kV, the area is 0.61 J, which represents the initial energy accumulation within the gap. As the voltage rises to 10.16 kV, the area increases to 0.71 J, suggesting that a higher voltage leads to a greater distribution of energy across the area. This trend continues at 10.94 kV, where the area expands to 0.94 J, and further at 11.73 kV, where the area reaches 0.96 J. As the voltage is increased beyond 12 kV, the area shows a more significant expansion. For instance, at 12.51 kV, the area is 1.10 J, and it continues to grow to 1.27 J at 13.29 kV. The increase in area becomes even more pronounced at higher voltages, with the area reaching 1.42 J at 14.08 kV and 1.53 J at 14.85 kV. At the highest voltages, the area undergoes substantial expansion. At 15.64 kV, the area is 1.79 J, and at 16.42 kV, it increases significantly to 2.21 J. Finally, at 17.20 kV, the area reaches 2.40 J, marking the peak of energy distribution within the gap. This suggests that as voltage increases, not only does the energy increase, but it also spreads over a larger area within the gap.

The relationship between voltage and area in figure 2, highlights the impact of voltage on the distribution and concentration of energy within the system. As voltage rises, the area influenced by the energy becomes larger, indicating more extensive energy distribution and potentially greater interactions within the system. The corresponding Lissajous figures for these conditions would likely show increasingly complex patterns as the area expands, reflecting the more intricate phase and amplitude interactions occurring at higher voltages and larger energy distributions.

Figure 3 shows that I-V characteristic and its corresponding Lissajous figure at 1 mm gap at various applied voltages reveals a clear trend of increasing area with rising voltage, reflecting the growing energy distribution within the gap. Starting at 9.38 kV, the area is 0.76 J, which increases to 1.035 J at 10.16 kV and 1.19 J at 11.73 kV. As the voltage continues to rise, the area expands further, reaching 1.30 J at 12.51 kV and 1.58 J at 13.29 kV. At higher voltages, the area continues to increase significantly, with values of 1.70 J at 14.07 kV, 1.76 J at 14.85 kV, and 2.17 J at 15.64 kV. The trend culminates at 2.59 J when the voltage reaches 17.20 kV. This progression indicates that as voltage increases, the energy spreads over a larger area within the 1 mm gap, suggesting more extensive energy interactions within the system. The corresponding Lissajous figures would likely show increasingly complex patterns, reflecting these enhanced interactions at higher voltages.

Figure 4 shows I-V characteristics with corresponding Lissajous figure at a 0.5 mm gap at varying applied voltages illustrates the relationship between voltage and the corresponding area, which represents the energy accumulation within the gap. As the voltage increases, the area grows significantly, indicating a direct correlation between the applied voltage and energy distribution. At 9.38 kV, the area is 0.84 J, showing the initial energy distribution within the gap. As the voltage rises to 10.17 kV, the area expands to 1.24 J, and further to 1.54 J at 10.95 kV, reflecting a steady increase in energy. This trend continues as the voltage reaches 11.73 kV, with the area growing to 1.94 J.

As the voltage continues to increase, the area expands more significantly. At 12.51 kV, the area reaches 2.23 J, and at 13.29 kV, it increases to 2.61 J. This trend persists at higher voltages, with the area reaching 2.67 J at 14.08 kV and 3.11 J at 14.86 kV. At the highest voltages, the area undergoes

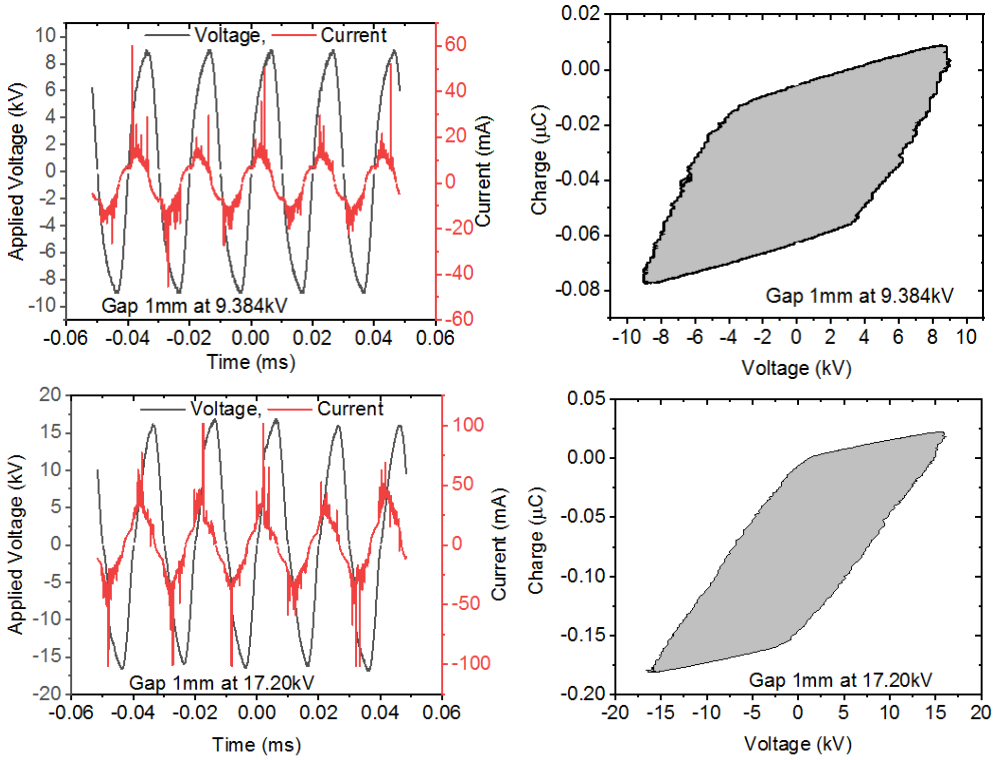

Figure 3. I-V characterization with corresponding Lissajous figure at 1.0 mm gap.

substantial growth. The area is 3.14 J at 15.64 kV, and it further increases to 3.74 J at 16.42 kV. Finally, at 17.25 kV, the area reaches its peak at 3.79 J. This steady increase in area as voltage rises suggests a growing energy concentration and distribution within the 0.5 mm gap.

Effect of voltage on electron density of coaxial DBD configuration

The relationship between the applied voltage and electron density is shown in figure 5 of coaxial DBD at different gap. As the voltage increases from 9.38 kV to 17.20 kV,

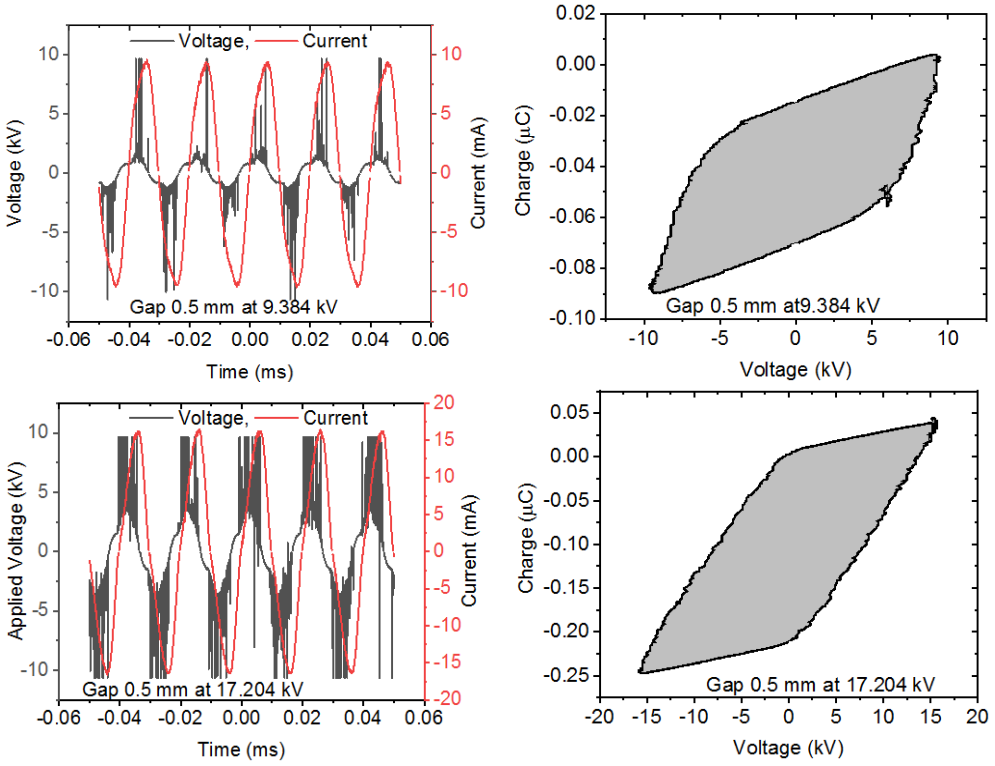

Figure 4. I-V characterization with corresponding Lissajous figure at 0.5 mm gap.

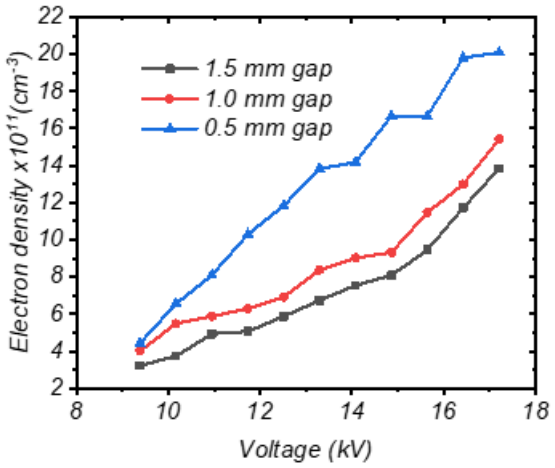

Figure 5. Electron density with voltage at different gap.

there is a corresponding rise in electron density for all gap distances. This is because higher voltages provide more energy to ionize the gas within the gap, generating more free electrons and ions, thereby increasing the overall electron density. For instance, at a 1.5 mm gap, the electron density increases from 3.23×10^{17} m^{-3} at 9.38 kV to 13.85×10^{17} m^{-3} at 17.20 kV. The electron density almost quadruples as the voltage nearly doubles, showing a nonlinear relationship between these two variables.

The gap size significantly influences the electron density for a given voltage. Smaller gaps produce higher electron densities because the electric field strength is inversely proportional to the gap distance. This means that as the gap narrows, the electric field becomes stronger, enhancing the ionization process and increasing electron density. At 10.95 kV, for example, the electron density is 4.94×10^{17} m^{-3} for a 1.5 mm gap, but it rises to 8.1×10^{17} m^{-3} for a 0.5 mm gap at the same voltage. This shows that smaller gaps lead to a more effective ionization process. For each voltage level, the electron density increases as the gap decreases. For example, at 14.08 kV, the electron density for a 1.5 mm gap is 7.55×10^{17} m^{-3}, whereas for a 0.5 mm gap, it rises to 14.18×10^{17} m^{-3}, nearly double the value for the 1.5 mm gap. This trend holds true across all voltage levels. The strongest impact is observed at the highest voltage of 17.20 kV, where the electron density reaches 20.09×10^{17} m^{-3} for the 0.5 mm gap, compared to 15.43×10^{17} m^{-3} for the 1 mm gap and 13.85×10^{17} m^{-3} for the 1.5 mm gap. As the voltage approaches and exceeds 14 kV, the electron density begins to increase at a faster rate, especially for the smaller gaps. For instance, between 13.29 kV and 14.08 kV, the electron density for the 0.5 mm gap jumps from 13.84×10^{17} m^{-3} to 14.18×10^{17} m^{-3}, and then continues to rise sharply, reaching 20.09×10^{17} m^{-3} at 17.20 kV. This rapid increase suggests a threshold voltage beyond which ionization becomes significantly more efficient, especially in smaller gaps where the electric field strength is already higher.

The results from this observation have important implications for designing and operating DBD systems. For applications requiring high electron densities, such as plasma generation, smaller gaps (like the 0.5 mm gap) and higher voltages are more effective. However, this must be balanced with the increased risk of electrical breakdown and thermal stress in the system at higher electron densities. For instance, the electron density at 17.20 kV with a 0.5 mm gap is more than 6 times higher than at the lowest voltage with a 1.5 mm gap, indicating that gap size and voltage can be tuned to achieve desired electron densities. Also, both applied voltage and gap size play crucial roles in determining the electron density in coaxial dielectric barrier discharge systems. Higher voltages and smaller gap sizes result in significantly higher electron densities. This is due to the stronger electric fields generated in smaller gaps, which enhance ionization and increase electron density. For practical purposes, understanding the interplay between these factors is essential for optimizing DBD systems, particularly for applications in plasma technology and material processing.

Effect of voltage on power consumption of coaxial DBD configuration

The power consumption increases as the applied voltage rises, similar to the previous electron density trends as shown in figure 6. As the voltage increases from 9.38 kV to 17.20 kV, power consumption increases significantly for all gap sizes. For instance, at a 1.5 mm gap, the power rises from 30.45 W at 9.38 kV to 126.38 W at 17.20 kV, which shows that power consumption quadruples as the voltage increases by approximately 80%. This increase in power consumption is expected due to the higher energy required to sustain the increased electron density at higher voltages. The gap distance also has a substantial effect on power consumption. Smaller gaps consistently lead to higher power consumption for the same voltage level. For example, at 12.51 kV, the power for the 1.5 mm gap is 55.5 W, while it is 111.6 W for the 0.5 mm gap. This nearly doubles the power requirement, emphasizing that the smaller gaps produce stronger electric fields, which require more energy to maintain the ionization process within the dielectric barrier discharge (DBD) system.

For every voltage, the power consumption follows the same pattern: it is the lowest for the 1.5 mm gap and the highest for the 0.5 mm gap. For example, at 14.076 kV, the power for the 1.5 mm gap is 63.55 W, for the 1 mm gap it is 85.15

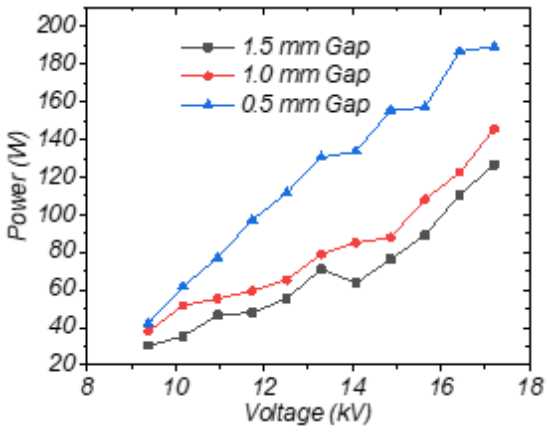

Figure 6. Power vs voltage with different gap of coaxial DBD.

W, and for the 0.5 mm gap it is 133.65 W. This reflects the stronger electric field in smaller gaps that consumes more power, even though the gap size is reduced. The difference in power consumption becomes more pronounced at higher voltages. A nonlinear increase in power consumption is observed, particularly in smaller gaps. At 11.73 kV, the power consumption for the 0.5 mm gap is 97.1 W, but by 17.20 kV, it jumps to 189.35 W-nearly doubling. For the 1 mm gap, the power increase is more gradual, from 59.45 W to 145.5 W over the same voltage range. This nonlinear behavior in smaller gaps indicates a more significant energy requirement to sustain the plasma at high voltages due to the increased ionization and electric field intensity.

From a practical perspective, higher power consumption in smaller gaps and at higher voltages can be both an advantage and a limitation, depending on the application of the DBD system. For processes that require high-energy plasma, smaller gaps and higher voltages may be necessary despite the higher power demands. For example, in material processing or surface modification applications, the 0.5 mm gap at 17.20 kV consumes 189.35 W, which could be ideal for maximizing plasma production. However, the high energy cost could pose a limitation for energy-sensitive applications. The power consumption in coaxial dielectric barrier discharge systems is directly influenced by both the applied voltage and the gap distance. Higher voltages and smaller gap distances result in significantly higher power consumption. The nonlinear relationship between power and voltage, especially in smaller gaps, suggests that careful optimization of these parameters is essential for achieving the desired plasma characteristics without unnecessary energy waste. Therefore, understanding this relationship can guide the design and operation of DBD systems for specific industrial applications.

Ozone production with time at different applied voltage

It's important to note that, even with some restrictions, the pattern shows a gradual increase in ozone generation over time. It was shown in the investigation that ozone production rose gradually over time. Nonetheless, an intriguing finding surfaced: The equipment employed in this investigation's ozone detecting capacity presented a limitation, since readings were not attainable within the first 25 seconds of operation. As a result, the ozone production graph started at the 25-second mark, meaning that data below this cutoff were not possible. This restriction emphasizes how crucial it is to comprehend the operational features and constraints of the apparatus in order to properly interpret experimental data. This tendency remarkably coincided with the results of the present study, indicating a continuous pattern of behavior in ozone formation. But it's important to note that the device utilized in this study has limits beyond 5 minutes, therefore the findings on ozone formation after this point cannot be compared to other studies that have conducted similar studies. Nonetheless, the initial 5-minute ozone production pattern was stable and comparable, suggesting that the behavior of ozone generation during this timeframe was consistent across trials. A more sophisticated comprehension of the dynamics of ozone production over time improves the interpretability and consistency of experimental results, enabling well-informed choices to be made regarding the optimization and application of ozone production.

In figure 7, the ozone production trend over time is depicted specifically for a 0.5 mm electrode gap configuration. This graph offers a detailed insight into how ozone generation evolves with increasing duration of operation. Notably, the data illustrates a consistent upward trend in ozone production over time. Additionally, it's observed that when the voltage is set at higher levels, the corresponding ozone production levels are also higher compared to setups with lower voltages, when considering ozone production at the same time intervals. This observation underscores the significant impact of applied voltage on ozone generation efficiency within the studied system. Furthermore, to ensure accurate measurement and reliable data interpretation, ozone production readings were taken after a 30-second interval following the initiation of ozone generation. Across the recorded time span, ozone production levels varied between 99 ppm to 786 ppm, with corresponding set voltages ranging from 9.38 kV to 17.20 kV. It's important to note that while taking ozone production readings at specific voltage settings, there was a margin of error of approximately ± 5 ppm inherent in the measurement function. However, despite this inherent variability, the graph indicates a near-constant trend in ozone production over time. This stability in ozone production levels suggests a consistent and reliable performance of the ozone generation system under the studied conditions, further affirming the robustness of the experimental setup. The analysis provides valuable insights into the intricate relationship between electrode gap distance, applied voltage, and ozone production dynamics over time, contributing to a comprehensive understanding of plasma-based ozone generation processes.

A fixed electrodes gap distance of 0.5 mm is used investigation of the generation of ozone at different constant voltage levels. The relation between applied voltage with ozone production is indicated by the fact that each voltage setting correlates to a particular range of the concentration of ozone (in parts per million). The ozone concentration varies from

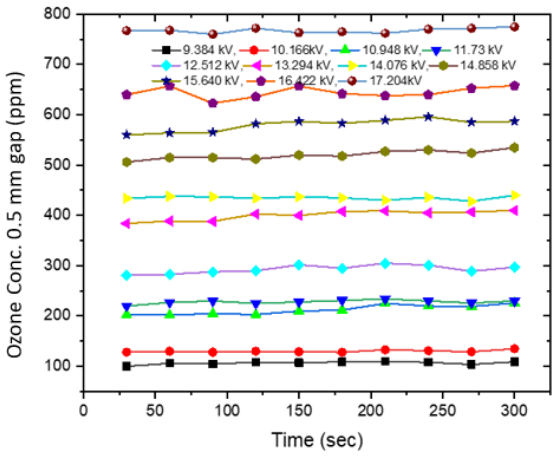

Figure 7. Ozone production at different applied voltage with time at 0.5 mm gap.

99 ppm to 102 ppm, with a starting voltage of 9.38 kV. An increasing tendency in the concentration of ozone is noticed when the voltage increases step by step. As an example, the ozone concentration ranges from 775 ppm to 786 ppm, the greatest range in the dataset, at 17.20 kV. According to the findings, there is a definite positive association between applied voltage with ozone formation, with greater voltages leading to higher concentrations of ozone. This relationship shows that the plasma system receives more energy input at higher voltages, which results in more effective ozone production processes. Furthermore, information about the susceptibility of the generation of ozone to voltage variations is provided by the measured ranges of concentrations of ozone at each voltage level. For example, very small increases in ozone concentration (99 ppm to $140-145$ ppm) are observed with smaller voltage increments (9.38 kV to 10.17 kV). There is a nonlinear connection between voltage as well as ozone production efficiency, yet, as the voltage increases and the pace of increase in concentrations of ozone becomes more noticeable.

In figure 8, the ozone production trend over time is depicted for a 1.0 mm electrode gap configuration. This graph provides a detailed illustration of how ozone generation evolves with increasing duration of operation. Similar to the observations in figure 43, it's evident that ozone production increases steadily over time, regardless of the electrode gap distance. Moreover, a clear correlation between applied voltage and ozone production is observed, wherein higher voltages correspond to higher ozone production levels when comparing ozone production at the same time intervals. This reaffirms the significance of applied voltage in influencing the efficiency of ozone generation within the studied system. To ensure accuracy and reliability, ozone production readings were consistently taken after a 30-second interval following the initiation of ozone generation. Across the recorded time span, ozone production levels varied between 30 ppm to 555 ppm, with corresponding set voltages ranging from 9.38 kV to 17.20 kV. Despite the inherent variability associated with ozone production measurements (approximately ± 5 ppm), the graph illustrates a remarkable consistency in ozone production levels over time. This stable trend further underscores the reliability and robustness of the experimental setup in generating ozone. The detailed analysis of ozone production at constant voltage levels and varying electrode gap distances offers valuable insights into the intricate interplay between these parameters and ozone generation dynamics. By understanding how different experimental conditions affect ozone production, researchers can optimize system parameters to achieve desired ozone concentrations for specific applications.

A thorough examination of the generation of ozone at several constant voltages with a fixed electrodes gap spacing of 1.0 mm. Each voltage setting represents a range of ozone concentrations (measured in parts per million), showing how applied voltage along with ozone production are related. The voltage spans from 9.38 kV to 56 ppm, with ozone concentrations in between. The concentration of ozone is consistently trending higher as the voltage rises step by step. For example, the ozone concentration hits its maximum range in the dataset at 17.20 kV, ranging from 550 ppm to 555 ppm. The applied voltage and ozone production are positively correlated, according to the data, with higher voltages producing higher quantities of ozone. This relationship emphasizes how crucial voltage regulation is to maximizing the production of ozone. Additionally, the ranges of concentrations of ozone that have been recorded at every voltage level shed light on how sensitive ozone formation is to voltage variations. For example, ozone concentration increases (from 40 ppm to $57-91$ ppm) comparatively moderately with lesser voltage changes (9.38 kV to 10.17 kV). The rate of rise in ozone concentration, however, sharpens with increasing voltage, suggesting a non-linear connection between voltage as well as ozone production efficiency. The trend in ozone production over time for an electrode gap arrangement of 1.5 mm is shown in figure 9. The graph shows that as operation time increases, ozone production rises steadily. When examining the generation of ozone at comparable time intervals, greater applied voltage setups are shown to produce more ozone than lower voltage setups, which is consistent with the findings in earlier figures. Readings of ozone production were obtained 30 seconds after the start of ozone creation. Ozone production

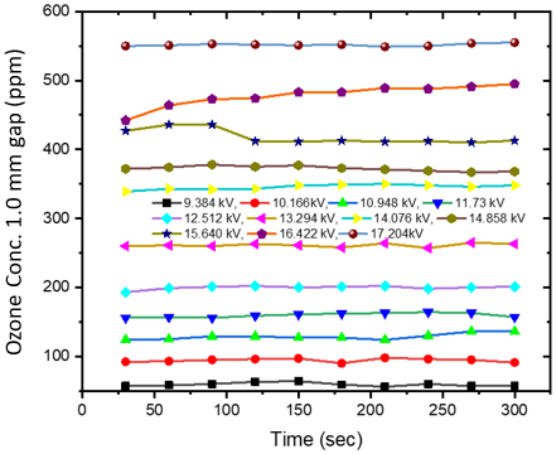

Figure 8. Ozone production at different applied voltage with time at 1.0 mm gap

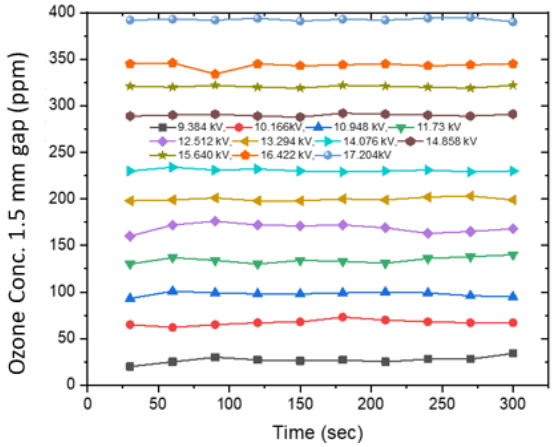

Figure 9. Ozone production at different applied voltage with time at 1.5 mm gap.

levels varied from 20 ppm through 395 ppm throughout the course of the recorded period, while associated set voltages varied from 9.38 kV through 17.20 kV. The graph shows a nearly consistent tendency in ozone production levels throughout time, despite the inherent variation connected to ozone production data (about ±5 ppm).

The data on ozone production at different fixed voltage levels, with a fixed electrodes gap spacing of 1.5 mm. An examination of the correlation between the voltage being applied and ozone formation is made possible by the fact that each voltage setting correlates to a certain range of ozone concentration. The ozone concentration varies from 20 ppm to 34 ppm, with a starting voltage of 9.38 kV. There is a discernible trend of rising ozone concentration as the voltage being applied is increased progressively. For example, the ozone concentration ranges from 390 ppm to 395 ppm, the greatest range recorded in the dataset, at 17.20 kV. The observed rise in concentrations of ozone with increasing voltage levels highlights the important impact of applied voltage on the efficiency of ozone formation. Increased voltages cause the plasma system to receive more energy, which makes the processes involved in producing ozone more effective. Furthermore, the ranges of concentrations of ozone that have been recorded at each voltage level shed light on how sensitive ozone formation is to variations in applied voltage. More mild increases in concentrations of ozone are caused by smaller voltage steps, especially at lower voltage levels. There is a non-linear relationship among voltage as well as ozone production efficiency, yet, as the voltage increases and the pace of increase in the concentration of ozone becomes more noticeable.

Interactions between electrode separation distance, applied voltage, along with ozone production efficiency are revealed through a comparative analysis of ozone production trends at three different electrode gap distances: 0.5 mm, 1 mm, and 1.5 mm. It is clear that the generation of ozone tends to decline with increasing electrodes gap distance at a specific voltage setting and ozone production time. The analysis of ozone formation at a distance of 1 mm between electrodes shows that ozone production rates rise gradually over time, and that greater voltages are associated with larger concentrations of ozone. Higher voltages allow for more energy to be input into the plasma reaction system, which leads to more effective ozone formation processes. This trend is consistent alongside the expected behavior.

Ozone production with different voltage at different gap

The current work reflects the constant pattern observed in Vaduganathan et al. [26] discussion of the behavior of ozone formation with applied voltage at varying airflow rates. In particular, it is found that ozone formation rises with increasing applied voltage at constant airflow rates of 2 LPM, 3 LPM, and 4 LPM. This implies that, independent of airflow rate, higher applied voltages lead to more effective ozone formation. Figure 10 delves more into the link between applied voltage and ozone formation at various distances between the electrodes. The graph shows that when electrode gap distance increases, ozone production reduces and increases with applied voltage. This finding holds true for

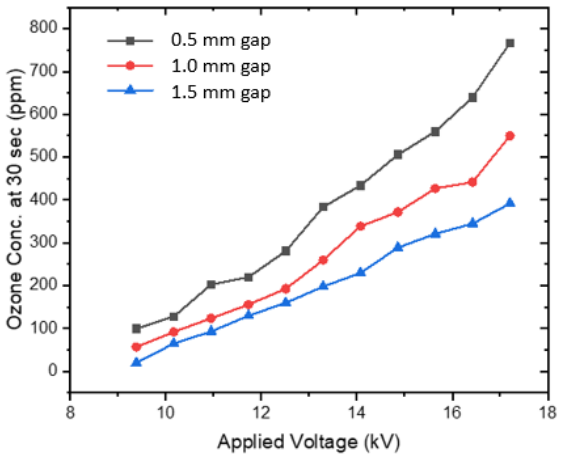

Figure 10. Ozone production with applied voltage at 30 sec with different gap.

other gap lengths, such as 1 mm, 2 mm, and 3 mm. The process of oxygen molecule splitting is responsible for the decrease in ozone formation with increasing gap distance. The applied voltage breaks the bonds between oxygen molecules more strongly at lower gap distances, which increases the rate of oxygen molecule splitting and, as a result, the generation of ozone. The energy needed to break these bonds, however, decreases as the gap distance rises, which lowers the efficiency of ozone generation. Figures 11 and 12 further illustrate the consistent structure of ozone formation with applied voltage over various electrode gap distances as well as time periods. This suggests that under various experimental conditions, the trends in ozone production that have been observed are stable and consistent. The results indicate that electrode gap distance affects the rate of oxygen molecule dissociation and, in turn, ozone formation, whereas applied voltage is a significant factor in ozone production efficiency. These discoveries advance our knowledge of the variables affecting plasma-based ozone generating and have the potential to influence the design and improvement of ozone production processes for a range of uses.

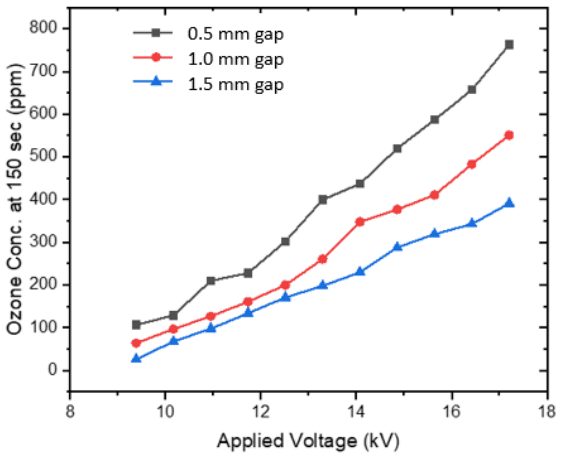

Figure 11. Ozone production with applied voltage at 150 sec with different gap.

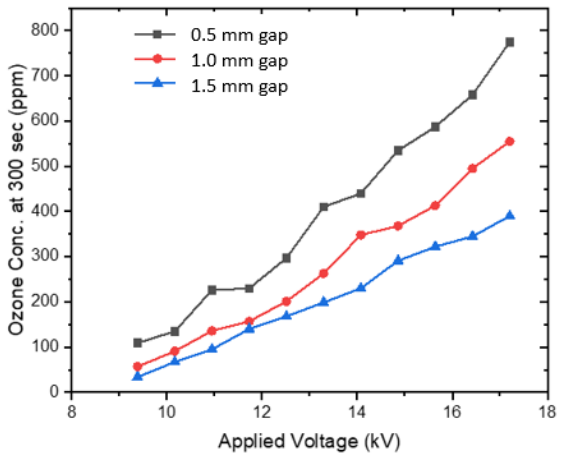

Figure 12. Ozone production with applied voltage at 300 sec with different gap.

A similar tendency is seen when ozone production lasts for 150 and 300 seconds, respectively. The formation of ozone is maximum at the shortest electrodes gap separation of 0.5 mm as well as diminishes as the gap distance increases. For instance, at spacing distances of 0.5 mm, 1.0 mm, along with 1.5 mm, respectively, the amount of ozone produced is 437 ppm, 348 ppm, along with 232 ppm at 150 seconds. Similarly, for gap distances of 0.5 mm, 1.0 mm, and 1.5 mm, respectively, ozone production is 535 ppm, 368 ppm, and 291 ppm at 300 seconds. The data supplied shows the levels of ozone formation for a constant applied voltage of 14.08 kV at various electrode gap spacing (0.5 mm, 1.0 mm, and 1.5 mm) and at various intervals (30 seconds, 150 seconds, and 300 seconds). It is found that ozone production reduces with increasing electrode gap distance at the initial time interval of 30 seconds. In particular, the production of ozone is most at 0.5 mm (434 ppm), lowest at 1.5 mm (230 ppm), and second highest at 1.0 mm (339 ppm). This pattern indicates that ozone production is more effectively produced at the beginning of the ozone generation process when the electrode gap distance is lower. This is probably because of a stronger electric field and higher rates of oxygen molecule splitting. This steady trend implies that electrode gap distance has a long-lasting effect on ozone production. Because of the stronger electric field along with higher rates of oxygen molecule splitting, smaller electrode gap distances continue to enable more efficient ozone synthesis than larger gap distances. According to the findings, electrode gap distance plays a crucial role in ozone production efficiency and must be carefully optimised in plasma-based ozone generating systems in order to provide appropriate ozone concentrations for a range of applications.

4. Conclusion

This study establishes a clear correlation between applied voltage, electrode gap distance, and ozone production in plasma-based systems. It demonstrates that higher applied voltages lead to increased ozone concentrations, with larger voltages enhancing ozone generation efficiency. Additionally, the electrode gap distance plays a crucial role, as smaller gaps result in more effective ozone production due to stronger electric fields and increased oxygen molecule dissociation. The relationship between voltage and ozone concentration is non-linear, with larger voltage increments yielding more pronounced increases in ozone levels. Based on these findings, optimizing ozone production requires minimizing electrode gap distances and regulating voltage to balance energy input and ozone yield. This research provides valuable insights into the factors influencing ozone generation and offers guidance for enhancing ozone production efficiency in various practical applications. To optimize both energy consumption and ozone output, it is recommended to maintain a minimal electrode gap distance and adjust the applied voltage based on specific application requirements.

Authors Contribution
All the authors have participated sufficiently in the intellectual content, conception and design of this work or the analysis and interpretation of the data (when applicable), as well as the writing of the manuscript.

Availability of data and materials
The data that support the findings of this study are available from the corresponding author, upon reasonable request.

Conflict of interests
The authors declare that they have no known competing financial interests or personal relationships that could have appeared to influence the work reported in this paper.

References

[1] H. Jakob. "Development of scalable and exible non-thermal Dielectric Barrier Discharge systems for novel low-temperature plasma applications. ". *Doctoral dissertation, University of Southampton*, 2022. URL https://www.researchgate.net/publication/367127689_Development_of_scalable_and_flexible_non-thermal_Dielectric_Barrier_Discharge_systems_for_novel_low-temperature_plasma_applications.

[2] P. Vanraes, A. Nikiforov, A. Bogaerts, and C. Leys. "Study of an AC dielectric barrier single micro-discharge filament over a water film. ". *Scientific Reports*, **8**(1):10919, 2018. URL https://www.nature.com/articles/s41598-018-29189-w.

[3] A. Barjasteh, Z. Dehghani, P. Lamichhane, N. Kaushik, E. H. Choi, and N. K. Kaushik. "Recent progress in applications of non-thermal plasma for water purification, bio-sterilization, and decontamination.". *Applied Sciences*, **11**(8):3372, 2021. DOI: https://doi.org/10.3390/app11083372.

[4] B. Bharti, H. Li, Z. Ren, R. Zhu, and Z. Zhu. "Recent advances in sterilization and disinfection technology: A review.". *Applied Radiation and Isotopes*, **308**:136404, 2022. DOI: https://doi.org/10.1016/j.chemosphere.2022.136404.

[5] A. Mizuno. "Industrial applications of atmospheric non-thermal plasma in environmental remediation. ". *Plasma Physics and Controlled Fusion*, **49**:A1, 2007. DOI: https://doi.org/10.1007/s41742-024-00685-4.

[6] C. O. R. Okpala, G. Bono, A. Abdulkadir, and C. U. Madumelu. "Ozone (O_3) process technology (OPT): An exploratory brief of minimal ozone discharge applied to shrimp product.". *Energy Procedia*, **75**:2427–2435, 2015. DOI: https://doi.org/10.1016/j.egypro.2015.07.206.

[7] M. Manna and S. Sen. "Advanced oxidation process: a sustainable technology for treating refractory organic compounds present in industrial wastewater. ". *Environmental Science and Pollution Research*, **30**(10):25477–25505, 2023.
DOI: https://doi.org/10.1007/s11356-022-19435-0.

[8] R. M. Pathak, A. Jayanarasimhan, S. Nandi, and L. Rao. "Investigating flow-induced changes in coaxial cylindrical dielectric barrier discharge using equivalent circuit modelling and chemical workbench simulations". *Plasma Chem Plasma Process*, 2024.
DOI: https://doi.org/10.21203/rs.3.rs-4613797/v1.

[9] J. Mikeš, S. Pekárek, and O. Hanuš. "Combined effects of electrode geometry and airflow streamlines patterns on ozone production of a cylindrical dielectric barrier discharge. ". *Electrochemistry Communications*, **172**:107873, 2025.
DOI: https://doi.org/10.1016/j.elecom.2025.107873.

[10] M. Gromov, Y. Gorbanev, E. Vervloessem, R. Morent, R. Snyders, N. De Geyter, and A. Nikiforov. "Electrification of fertilizer production via plasma-based nitrogen fixation: A tutorial on fundamentals.". *RSC Sustainability*, **3**:757, 2025.
DOI: https://doi.org/10.1039/D4SU00726C.

[11] D. Korzec, F. Freund, C. Bäuml, P. Penzkofer, and S. Nettesheim. "Hybrid dielectric barrier discharge reactor: Characterization for ozone production. ". *Plasma*, **7**:585–615, 2024.
DOI: https://doi.org/10.3390/plasma7030031.

[12] C. Liang, Z. Liu, B. Sun, H. Zou, and G. Chu. "Improvement in discharge characteristics and energy yield of ozone generation via configuration optimization of a coaxial dielectric barrier discharge reactor.". *Chinese Journal of Chemical Engineering*, **60**:61–68, 2023.
DOI: https://doi.org/10.1016/j.cjche.2022.11.016.

[13] K. M. Ahmed, A. S. Barakat, M. Badawi, S. A. Ward, W. H. Gaber, and M. M. Darwish. "Ozone generation using high voltage atmospheric-pressure DBD reactor for sterilization processes. ". *24th International Middle East Power System Conference (MEPCON)*, pages 1–6, 2023.
DOI: https://doi.org/10.1109/MEPCON58725.2023.10462426.

[14] G. P. Panta, H. B. Baniya, S. Dhungana, D. P. Subedi, and A. Papadaki. "Ozone production in cylindrical Co-axial double dielectric Barrier discharge ozone generator.". *Walailak Journal of Science and Technology (WJST)*, **18**:9856–10, 2021.
DOI: https://doi.org/10.48048/wjst.2021.9856.

[15] X. Gou, D. Yuan, L. Wang, L. Xie, L. Wei, and G. Zhang. "Enhancing ozone production in dielectric barrier discharge utilizing water as electrode. ". *Vacuum*, **212**:102–112, 2023.
DOI: https://doi.org/10.1016/j.vacuum.2023.112047.

[16] R. Engeln, B. Klarenaar, and O. Guaitella. "Foundations of optical diagnostics in low temperature plasmas.". *Plasma Sources Science and Technology*, **29**:063001, 2020.
DOI: https://doi.org/10.1088/1361-6595/ab6880/meta.

[17] Environmental Protection Agency. "Wastewater technology fact sheet ozone disinfection.". *Journal of Inorganic and Organometallic Polymers and Materials*, 2023. URL https://www3.epa.gov/npdes/pubs/ozon.pdf.

[18] M. Remondino and L. Valdenassi. "Different uses of ozone: Environmental and corporate sustainability. Literature review and case study. ". *Sustainability*, **10**:4783, 2018.
DOI: https://doi.org/10.3390/su10124783.

[19] A. C. Babu and A. Jacob. "Chemistry of ozone processing. ". *Chemistry of Thermal and Non-Thermal Food Processing Technologies*, pages 289–311, 2025.
DOI: https://doi.org/10.1016/b978-0-443-22182-8.00014-0.

[20] M. Mahmoodi and E. Pishbin. "Ozone-based advanced oxidation processes in water treatment: recent advances, challenges, and perspective.". *Environmental Science and Pollution Research*, **32**:3531–3570, 2025.
DOI: https://doi.org/10.1007/s11356-024-35835-w.

[21] R. Snoeckx and A. Bogaerts. "Plasma technology-a novel solution for CO_2 conversion?". *Chemical Society Reviews*, **46**:5805–5863, 2017.
DOI: https://doi.org/10.1039/C6CS00066E.

[22] R. Shrestha, U. M. Joshi, and D. P. Subedi. "Experimental study of ozone generation by atmospheric pressure dielectric barrier discharge. ". *International Journal of Recent Research and Review*, **8**:24–30, 2015. URL https://www.ijrrr.com/papers8-4/paper4-Experimental.

[23] P. B. Khadka, S. Sharma, Y. P. Basel, G. Acharya, R. Shrestha, and D. P. Subedi. "Electrical and optical characterization of atmospheric pressure Co-axial dielectric barrier discharge (APDBD) used for ozone generation.". *Journal of Emerging Technologies and Innovative Research*, **6**:93–94, 2019. URL https://www.researchgate.net/profile/Rajendra-Shrestha/publication/334836033_Electrical_and_Optical_Characterization_of_Atmospheric_Pressure_Co-axial_Dielectric_Barrier_Discharge_APDBD_Used_for_Ozone_Generation/links/5d42e0a5299bf1995b5bf349/Electrical-and-Optical-Characterization-of-Atmospheric-Pressure-Co-axial-Dielectric.pdf.

[24] A. Yehia. "Consumption of the electric power inside silent discharge reactors. ". *Physics of Plasmas*, **22**:1–8, 2015.
DOI: https://doi.org/10.1063/1.4905708.

[25] T. C. Manley. "The electric characteristics of the ozonator discharge.". *Transactions of The Electrochemical Society*, **84**:1–6, 1943.
DOI: https://doi.org/10.1149/1.3071556.

[26] L. Vaduganathan, B. A. Poonamallie, and M. Nagalingam. "Effects of temperature and flow rates of ozone generator on the DBD by varying various electrical parameters. ". *American Journal of Applied Sciences*, **9**:1496–1502, 2012.
DOI: https://doi.org/10.3844/ajassp.2012.1496.1502.

[27] D. P. Subedi, R. P. Guragain, and U. M. Joshi. "Surface modification of polymers by 50 Hz dielectric barrier discharge (DBD) plasma produced in air at 40 Torr.". *Fundamental Plasma Physics*, **10**: 100058, 2024.
DOI: https://doi.org/10.1016/j.fpp.2024.100058.

[28] D. P. Subedi, U. M. Joshi, C. S. Wong, and R. S. Rawat. "Dielectric barrier discharge (DBD) plasmas and their applications. In: Plasma Science and Technology for Emerging Economies. ". *Fusion Science and Technology*, pages 693–737, 2017.
DOI: https://doi.org/10.1007/978-981-10-4217-1_13.

[29] R. B. Tyata, D. P. Subedi, R. Shrestha, and C. S. Wong. "Generation of uniform atmospheric pressure argon glow plasma by dielectric barrier discharge.". *Pramana - Journal of Physics*, **80**:507, 2013.
DOI: https://doi.org/10.1007/s12043-012-0494-z.